GENERATION AND RETENTION OF HELIUM AND HYDROGEN IN AUSTENITIC STEELS IRRADIATED IN A VARIETY OF LWR AND TEST REACTOR SPECTRAL ENVIRONMENTS - F. A. Garner, B. M. Oliver, L. R. Greenwood, D. J. Edwards and S.M. Bruemmer (Pacific Northwest National Laboratory)* M. L. Grossbeck, (Oak Ridge National Laboratory)

OBJECTIVE

The purpose of this effort is to explore the possibility that both helium and hydrogen influence the behavior or stainless steels during neutron irradiation.

SUMMARY

In fission and fusion reactor environments stainless steels generate significant amounts of helium and hydrogen by transmutation. The primary sources of helium are boron and nickel, interacting with both fast and especially thermal neutrons. Hydrogen arises primarily from fast neutron reactions, but is also introduced into steels at often much higher levels by other environmental processes. Although essentially all of the helium is retained in the steel, it is commonly assumed that most of the hydrogen is not retained. It now appears that under some circumstances, significant levels of hydrogen can be retained, especially when helium-nucleated cavities become a significant part of the microstructure.

A variety of stainless steel specimens have been examined from various test reactors, PWRs and BWRs. These specimens were exposed to a wide range of neutron spectra with different thermal/fast neutron ratios. Pure nickel and pure iron have also been examined. It is shown that all major features of the retention of helium and hydrogen can be explained in terms of the composition, thermal/fast neutron ratio and the presence or absence of helium-nucleated cavities. In some cases, the hydrogen retention is very large and can exceed that generated by transmutation, with the additional hydrogen arising from either environmental sources and/or previously unidentified radioisotope sources that may come into operation at high neutron exposures.

INTRODUCTION

It is well known that helium and hydrogen are formed in stainless steels, as well as in other metals and alloys, by neutron-induced transmutation. Hydrogen is also introduced into metals during irradiation by a variety of other mechanisms. Examples are corrosion, recoil injection of protons after neutron-water collisions, radiolytic decomposition of water in light water reactors, and the equilibrium dissociation arising from hydrogen overpressures used in PWRs. Although essentially all of the helium is retained in the steel, it is commonly assumed that most of the hydrogen cannot be retained at high concentrations and will therefore diffuse out of the steel.

Both of these gases are known to exert deleterious effects on the properties of stainless steels, but two potential degradation processes are of current interest. First, it is well known that helium and other gases stabilize small vacancy clusters to form bubbles and void cavities, and thereby accelerate the onset of void swelling. It has recently been suggested that hydrogen may possibly serve a similar role [1]. Second, hydrogen has also been

---

* Pacific Northwest National Laboratory (PNNL) is operated for the U.S. Department of Energy by Battelle Memorial Institute under contract DE-AC06-76RLO-1830.

occasionally suggested to play a role in irradiation-assisted stress corrosion cracking, but no convincing evidence of hydrogen's direct role has yet been provided.

To date no systematic attempt has been made to measure the concentrations of both gases in highly neutron-irradiated stainless steels, or to investigate the possible interaction of the two gases. This paper first presents a summary of such measurements on a variety of stainless steel specimens irradiated in PWRs and BWRs. Second, a series of specimens from several test reactors are used to address specific questions arising from the LWR results. The specimens examined in these two groups were therefore exposed to a wide range of neutron spectra. Third, and finally, pure nickel and pure iron wires used as dosimeters and irradiated in HFIR were also measured to address issues related to transmutation sources of helium and hydrogen.

Transmutant sources of helium and hydrogen

Virtually all elements in stainless steel produce helium to some degree during neutron irradiation via (n,α) reactions with neutrons with energies above ~4 MeV. The majority of the helium from such reactions is formed from the five isotopes of natural nickel (primarily ^{58}Ni), with all other major elements typically used in steels having much smaller cross sections [2]. The range of alpha particles from this type of reaction is rather small, typically less than a micron, leading to minimal energetic losses across the specimen surfaces.

Helium is also formed by interactions with low energy or thermal neutrons that exist at high fluxes in water-moderated reactors. There are two important reactions of this type. The first is the (n,α) reaction with ^{10}B, which comprises 19.9% of natural boron. This contribution to helium production is generally quite small (<<50 appm) and normally saturates quickly with the rapid burnout of this isotope in most reactor neutron spectra having a significant thermal component. Note that ^{6}Li also has a higher thermal neutron (n,α) cross-section, but ^{6}Li comprises ~7% of natural lithium, however, and lithium is generally not a significant impurity in steel.

The second major contribution arises from the ^{58}Ni(n,γ) ^{59}Ni (n,α) reaction sequence, which is essentially unsaturable within the range of conditions relevant to LWRs and fusion devices [3]. ^{59}Ni is a radioactive isotope not found in natural nickel. It is important to note that this two-step generation reaction is non-linear with exposure, involving the buildup of ^{59}Ni as the first step. Therefore, this contribution exhibits a delay in its production and continuously accelerates in rate with increasing exposure, only saturating at thermal neutron fluences $>10^{23}$n/cm^{2}, well above the range of LWR and fusion interest. Most importantly, the degree of acceleration is directly proportional to the thermal-to-fast neutron ratio, which can vary strongly with position both within and especially outside of LWR cores. The thermal-to-fast ratio increases strongly as the local water to fuel (or metal) ratio increases. Usually there is a strong increase in the ratio just outside the core boundary. Both within and especially outside of LWR cores, this contribution soon becomes the dominant source of helium in nickel-bearing alloys.

Both of these thermal neutron reactions are very exothermic and yield energetic helium atoms with ranges on the order of several microns. Therefore the energetic losses of helium across specimen surfaces are somewhat larger. For samples with minimum dimensions comparable to the recoil distance, the near-surface regions of specimens must be removed before measurement of helium proceeds.

Helium is both very immobile and chemically inert. Therefore it has no driving force for significant diffusional migration or segregation, leading to near total trapping within the specimen. Since it does not further transmute, it can be used as a fluence and spectral monitor for retrospective dosimetry. This means that an estimation of the neutron exposure can be made for specimens whose exposures are not well known, especially when other measurements are also used that measure radioactivation or isotopic shifts for selected elements.

Hydrogen is also generated by transmutation, but it is important to remember that hydrogen can be introduced into steels by other environmental processes. Examples are corrosion, radiolytic decomposition of water, direct injection from proton recoil following collisions of neutrons with the H in water, and from equilibrium dissociation of the hydrogen overpressure maintained in PWR reactors. Another example arises from diffusion of transmutant hydrogen produced at large levels in adjacent materials.

In steels, hydrogen arising from transmutation is formed primarily from the various nickel isotopes, especially ^{58}Ni, interacting with fast neutrons above ~1 MeV. The production rate via this reaction is essentially linear with accumulating exposure. Other constituents of typical steels also generate hydrogen by (n,p) reactions, but the cross sections are much smaller than those of nickel. Due to the lower (n,p) threshold (1 MeV) compared to the ~4 MeV threshold for alpha production, the H/He ratio due to fast neutrons is usually on the order of 14-20, depending on the details of the fast portion of the neutron spectra. However, there is also a ^{58}Ni(n,γ) ^{59}Ni(n,p) reaction, with a thermal cross section that is about one-sixth of the ^{59}Ni helium production cross section [4]. The total hydrogen production rate in nickel-bearing alloys is therefore also non-linear with increasing exposure, but at only 1/6th the rate of helium.

Hydrogen is thought to be very mobile in steels at LWR-relevant and fusion-relevant temperatures, and therefore it might be expected that very little would be retained. There is some evidence, however, that hydrogen can be stored in highly irradiated steels under certain conditions [1, 5]. In particular, hydrogen retention appears to be accelerated when large amounts of helium are cogenerated [1]. More importantly, hydrogen arising from non-transmutation sources might also be stored. This is a particularly important consideration in LWRs with water coolant, but not necessarily in sodium-cooled fast reactors.

In summary, the major source of helium at high neutron exposure is nickel, and the production rate is proportional to the nickel content and the local thermal-to- fast neutron ratio, but in a non-linear manner with increasing exposure. Transmutant hydrogen is similarly dependent on the Ni content and the thermal- to-fast ratio, but the non-linearity is less pronounced due to the lower (n,p) thermal cross section. The production of helium by boron occurs very quickly, saturating at a rate that is strongly dependent on the thermal neutron flux.

Gas measurement procedures

Smaller sections on the order of milligrams were first cut from each sample. These sections were then etched to remove ~0.013 mm or more of surface material. This etching step was done to remove material that may have been affected by α-recoil either out of the sample or into the sample from adjacent materials during irradiation. After etching, smaller specimens were cut from each section for duplicate helium analysis. The specimens were cut using small wire cutters. Before each use, the cutters were cleaned by wiping several times with a dry lint-free paper cloth (Kimwipe). Replicate helium analyses are routinely performed to

give an indication of the analysis reproducibility and helium homogeneity in each sample. Prior to analysis, each specimen was cleaned in alcohol and air-dried. The mass of each specimen was determined to an accuracy of ±0.002 mg using a calibrated microbalance traceable to the National Institute of Standards and Technology (NIST).

The helium content of each specimen was determined by isotope-dilution mass spectrometry following vaporization in a resistance-heated graphite or tungsten-wire crucible in one of the mass spectrometer system's high-temperature vacuum furnaces [6,7]. The absolute amount of ^{4}He released was measured relative to a known quantity of added ^{3}He "spike". The helium spike was obtained by expanding and partitioning a known quantity of gas through a succession of calibrated volumes. The mass spectrometer was calibrated for mass sensitivity during each series of runs by analyzing known mixtures of ^{3}He and ^{4}He.

Hydrogen analyses were also conducted by gas mass spectrometry using a newly developed H analysis system [8]. The analysis procedure involved dropping the individual specimens, under vacuum, into a small cylindrical ceramic crucible heated to approximately 1200°C. During initial vacuum pumping, the sample chamber and crucible volume were subjected to a low-pressure (~200 mm Torr) argon gas discharge to aid in desorption of water or hydrated-oxide surface layers that could be dissociated by the hot crucible during analysis, and thus contribute to the measured H release. The sample chamber was then connected to the high-vacuum analysis chamber, and the analysis crucible was pre-heated to approximately 1000°C for several days. The crucible temperature was increased to 1200°C a few hours prior to analysis. During the pre-heating and subsequent analysis procedure, the sample chamber was maintained at room temperature.

Hydrogen release was measured as a function of time using a quadruple mass spectrometer connected to the analysis chamber. The total hydrogen was determined from the integral of the hydrogen release curve. Calibration of the system sensitivity was accomplished using a calibrated H leak source of ~1 x 10^{-10} mole H_2/sec, with a stated absolute uncertainty of ±15% (3σ). Calibration measurements were conducted before and after each sample analysis, and showed an overall standard deviation of ~2 to 3%. Measurements were also conducted on milligram-sized specimens of a standard hydrogen-containing steel maintained in the laboratory. Variability in numerous replicate measurements of this steel is currently averaging approximately 20% (1σ), and is believed to represent actual heterogeneity in the hydrogen content for these small samples.

<u>LWR specimens examined</u>

Four sets of LWR specimens were investigated. In the first set Types 304 and 316SS heats with previously characterized IASCC response were selected from an extensive ABB-Atom testing program [9]. In this program three different 304SS and three different 316SS heats were irradiated to dose levels of ~0.4 to 9 x 10^{21} n/cm^2 (~0.6 to 13.3 dpa) in a commercial BWR (Barsebäck) at a temperature of ~275°C. The compositions are shown in Table 1. A total of 38 specimen conditions were chosen to span the range of irradiation doses shown in Table 2. Unirradiated archive materials were also available for each heat.

The second LWR set of specimens examined were sections cut from two different locations of the top guide of the core shroud from the KWW Wurgassen BWR reactor. This component was constructed from Type 347 stainless steel, as described in Table 3. One specimen was extracted above the center of the core with an estimated fluence of 1.4 x 10^{21} n/cm^2 E>0.1 MeV (~2 dpa). The second, lower dose piece was obtained from another section away from the core center at an estimated fluence of 5 x 10^{19} n/cm^2 (~0.07 dpa).

Table 1. Bulk compositions of ABB-Atom heats, wt%

	304-B	**304-C**	**304-E**	**316-F**	**316-K**	**316-P**
C	0.035	0.014	0.015	0.009	0.055	0.040
Cr	18.3	18.6	18.5	16.7	16.5	16.7
Ni	8.5	10.2	10.9	11.6	12.4	12.2
Mo	0.4	0.3	0.1	2.7	2.3	2.6
Mn	1.4	1.3	0.8	1.4	1.7	1.8
Si	0.65	0.43	0.05	0.26	0.64	0.59
P	0.031	0.023	0.006	0.021	0.016	0.024
S	0.029	0.006	0.009	0.001	0.006	0.007
B	<0.0004	<0.0004	<0.0004	0.0010	<0.0004	0.0013
N	0.067	0.077	0.039	0.062	0.029	0.058

Table 2. CIR Materials from the ABB-Atom IASCC Program, indicating Sample Numbers and Dose Conditions (n/cm^2, E>1MeV)

304SS Heat B	304SS Heat C	304SS Heat E	316SS Heat F	316SS Heat K	316SS Heat P
#B15 0.5×10^{21}	#C36 0.4×10^{21}				
#B27 0.8×10^{21}	#C35 0.6×10^{21}	#E6 0.8×10^{21}	#F6 0.8×10^{21}	#K4 0.7×10^{21}	#P28 0.8×10^{21}
#B21 1.1×10^{21}	#C5 1.2×10^{21}	#E1 1.2×10^{21}	#F1 1.1×10^{21}	#K3 1.1×10^{21}	#P14 1.1×10^{21}
#B74 2.2×10^{21}	#C69 2.5×10^{21}	#E18 2.2×10^{21}	#F12 2.3×10^{21}	#K10 2.6×10^{21}	#P64 2.0×10^{21}
#B79 3.4×10^{21}	#C62 3.4×10^{21}	#E15 3.1×10^{21}	#F10 3.3×10^{21}	#K9 4.0×10^{21}	#P51 3.4×10^{21}
#B132 5.9×10^{21}	#C106 5.8×10^{21}	#E24 6.0×10^{21}	#F16 6.6×10^{21}	#K18 5.0×10^{21}	#P79 5.5×10^{21}
#B124 9.2×10^{21}	#C87 9.3×10^{21}	#E22 9.0×10^{21}	#F15 9.0×10^{21}	#K15 9.3×10^{21}	#P83 9.2×10^{21}

The third set of LWR specimens were several heats of 304 and 348 stainless steels irradiated in the control rod guide tube of a standard 14X14 fuel assembly of the KWO Obrigheim PWR as part of a swelling-mandrel test program [10]. It is important to note that the B_4C in these mandrels probably lowered the thermal-to-fast neutron ratio significantly,

Table 3. Composition and fabrication history of the top guide for the Wurgassen KWW Nuclear Power Plant

Heat # 71836			Semi-finished Product (Solution Annealed 1020°C/WQ) Room Temperature Tensile Properties					Stabilization Ratio Nb/C
			0.2%YS	UTS	%TE	%RA		
			295 MPa	630 MPa	50.7	60.7		10
Measured Bulk Chemistry (wt%)								
C	Si	P	S	Cr	Mn	Fe	Ni	Nb + Ta
0.049	0.65	0.02	0.014	18.4	1.3	68.5	10.6	0.49

and thereby the ^{59}Ni helium production. This complication does not allow us to specify the thermal neutron spectrum very accurately.

The fourth set of LWR specimens were cut from a cold-worked 316 baffle bolt removed from the Tihange 1 PWR. While the major element composition is known, there is no knowledge of the boron content of this bolt. As shown in Figure 1, three sections were cut at 1, 25 and 55 mm from the bolt head surface, with doses of 19.5, 12.2 and 7.5 dpa, respectively, as determined by retrospective dosimetry. This bolt and its full characterization are presented in another paper in this symposium [5].

Results: LWR specimens

The measured helium values for the ABB and 304/308 PWR specimens are shown in Figure 2. Helium concentrations increase consistently with increasing dose for each heat. The rate

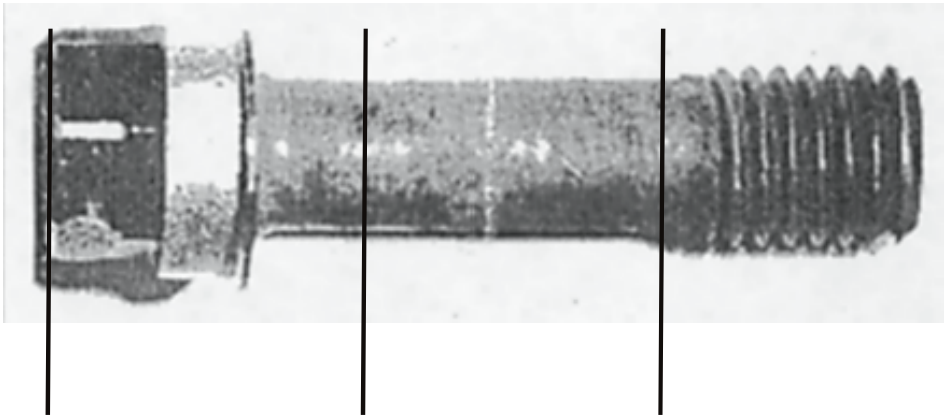

Bolt head 1 mm 320°C, 19.2 dpa | **Bolt shank 25 mm 343°C, 10 dpa** | **Near Threads 55 mm 333°C, 6 dpa**

Figure 1. Location of specimens cut from baffle bolt. The dpa levels have recently been revised to 19.5, 12.2 and 7.5 dpa based on retrospective dosimetry.

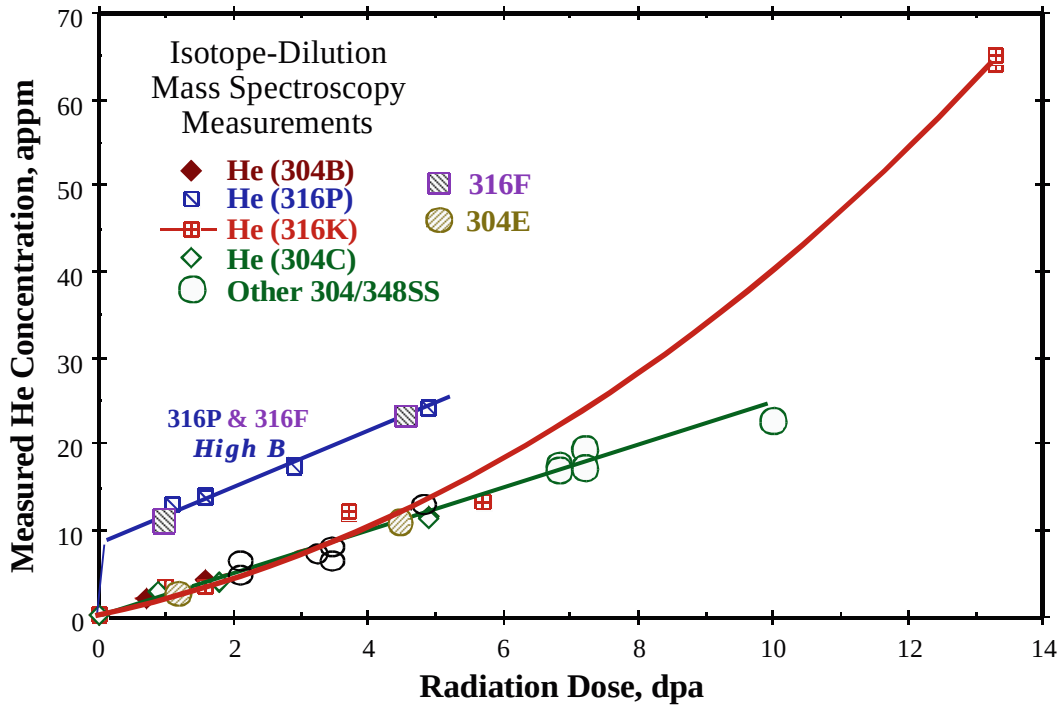

Figure 2. Helium concentrations measured in various 300 series stainless steels after irradiation in various LWRs.

of increase is approximately 2.5 appm per dpa for 316 heats until ~10 dpa. From fast neutron reactions only, the calculated helium generation rate is only about 1 appm/dpa, so the apparently linear 2.5 appm/dpa rate represents the combined effect of the time-varying boron, fast neutron and ^{59}Ni contributions. As expected, there is a more obvious acceleration in helium production rate indicated by heat K at high dose as the ^{59}Ni contribution continues to accelerate.

The largest difference among the ABB heats is seen for 316 heats P and F when compared with the others. Both of these heats show an initial offset in helium content (~10 appm) at the lowest dose investigated. This occurs due to higher boron levels in these two heats that burns out by ~1 dpa. Since ^{10}B comprises ~20% of natural boron, the bulk concentration of this element in heat P can be estimated to be ~55 appm, and ~40 appm in heat F. These numbers agree quite well with predicted values based on the bulk concentrations listed in Table 1.

The increasing rate of helium generation at high neutron exposure is consistent with the buildup of ^{59}Ni. The much lower rate of increase in the 304SS Heat B and 348SS PWR specimens most likely reflects both their lower nickel content compared to 316 heats and a lowering of the local thermal neutron flux by the B_4C inside the mandrels. The continued apparent linearity of helium generation at higher dpa is also consistent with a lower thermal neutron contribution.

Using a typical in-core LWR spectrum, and removing the boron contributions, it is possible to reproduce all features of the measured helium behavior, as shown in Figure 3. Only the

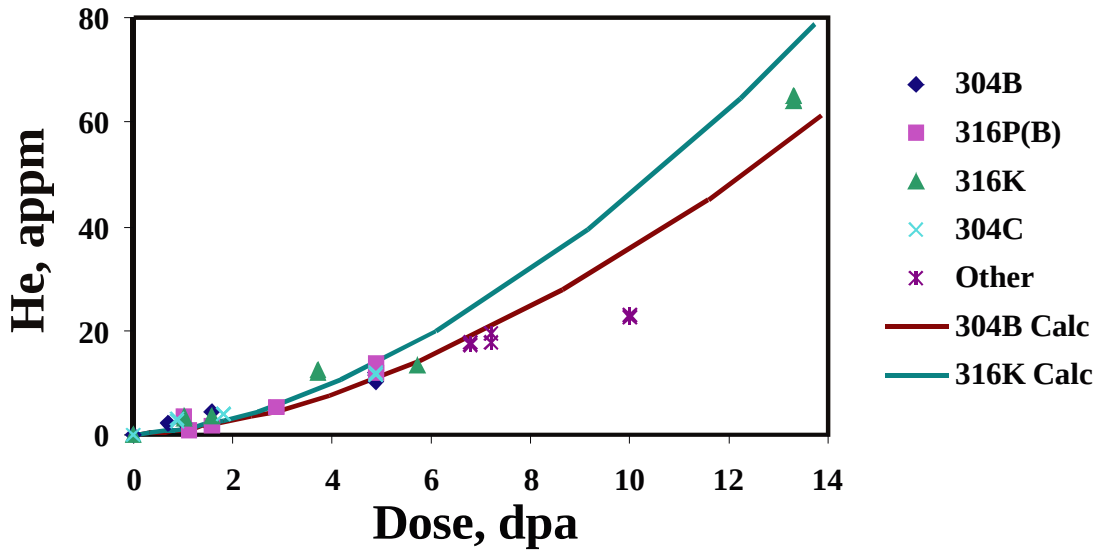

Figure 3. Comparison of predicted and measured helium levels after removal of boron contributions.

Obrigheim PWR data on 304/348 stainless fall below the prediction, as expected by the B_4C suppression of the local thermal neutron population.

With the exception of ABB heat C the retained hydrogen concentrations in the ABB heats shown in Figure 4 appear to be relatively low and perhaps increasing at a relatively low rate.

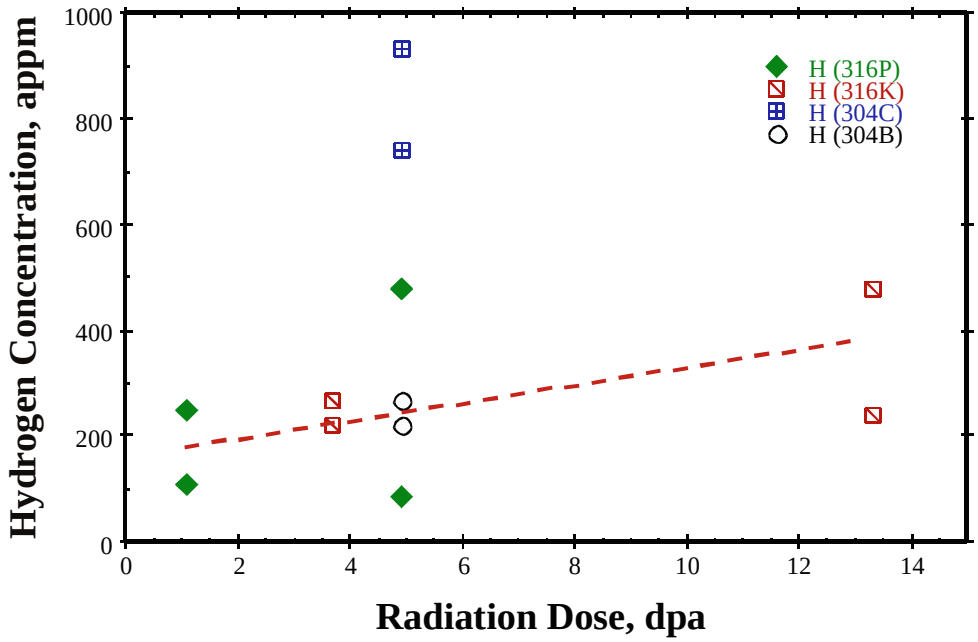

Figure 4. Hydrogen concentrations measured in ABB heats.

Using the same spectra employed for the helium above, calculations of the predicted concentrations of transmutation-induced hydrogen in the ABB specimens are significantly lower than those measured, indicating that environmental sources must be the dominant sources.

The helium measurements shown in Figure 5 compare the differences between the two Wurgassen conditions relative to the ABB-Atom materials. The much lower helium content at the 0.07 dpa condition compared to the 2 dpa condition is primarily due to the lower overall flux at this position. Compared to the ABB-Atom materials, the higher thermal-to-fast ratio in the out-of-core region produces significant increases in the He/dpa ratio. Although not as noticeable without close inspection of Figure 5, the 0.07 dpa condition also has a higher helium content than the low-boron ABB-Atom materials at comparable doses. The boron content of this material is unknown, however, so how much helium is derived from transmutation of ^{10}B cannot be predicted.

The hydrogen concentrations shown in Figure 6 are surprising in that, for reasons that remain unclear, the 0.07 dpa condition has much higher hydrogen than measured in the 2 dpa condition. Compared to the ABB-Atom materials, the Wurgassen plate appears to have higher hydrogen concentrations at both doses, but the concentration at 0.07 dpa exceeds that of the ABB-Atom materials by a significant margin.

Table 4 lists the results of the gas measurements on the Tihange bolt. Figure 7a shows the helium measured at three positions along the Tihange baffle bolt, with all data points connected to each other. At first glance, it appears that the data imply a very large level of boron in the steel, on the order of 150 appm. This is an incorrect conclusion, however, and is

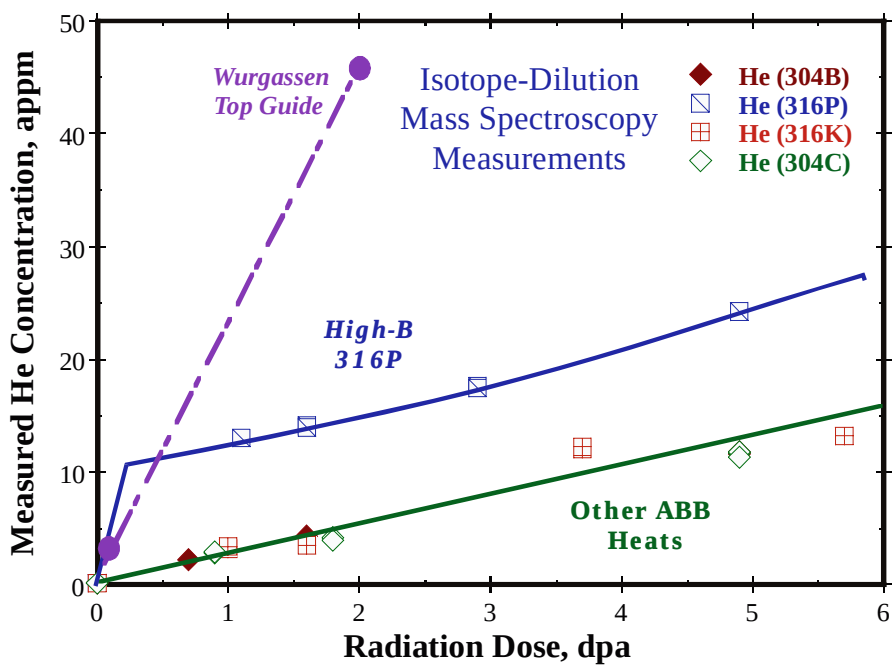

Figure 5. Helium concentration in two Wurgassen samples compared to those of the ABB materials.

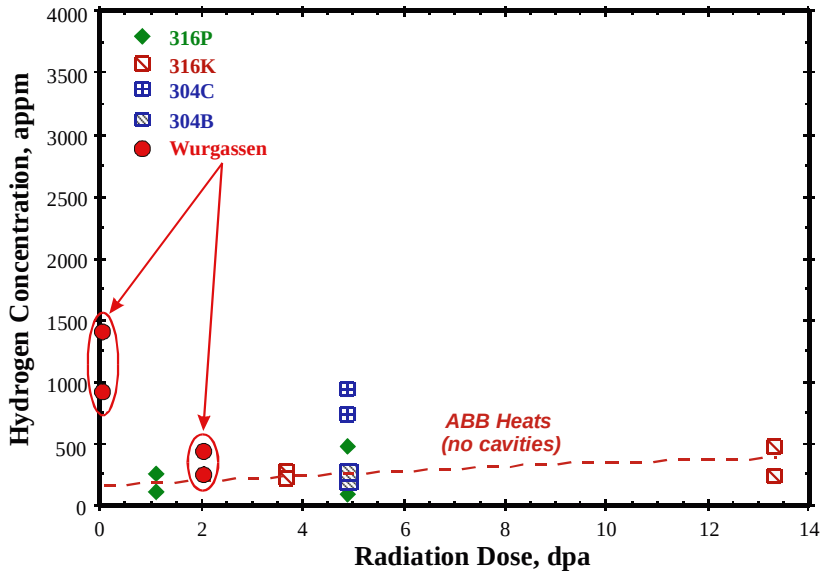

Figure 6. Hydrogen concentration in two Wurgassen samples compared to those of the ABB materials.

predicated on an assumption that the thermal-to-fast ratio is the same everywhere along the bolt axis.

Whereas the ABB heats occupied an in-core position without significant variations in thermal-to-fast ratio, the bolt head is only millimeters from a fuel element which absorbs thermal neutrons strongly, while the shaft of the bolt experiences a significant change in this ratio along the bolt axis as it penetrates into areas where water surrounds the former plate in which it is buried.

By using the known power history of the reactor, measuring the activity of ^{60}Co and ^{54}Mn, and also measuring the cobalt and iron compositions using EDXRF, the neutron exposure of these three bolt positions can be determined. Such a process is called retrospective dosimetry and was employed on this bolt. Dpa levels calculated with this procedure agree rather well (19.5 vs. 19.2 dpa at the bolt head surface) with calculated values provided by the Tihange vendor, Tractebel. Figure 8 shows that the thermal-to fast ratio increased about a factor of two between the 1 and 55 mm positions. Figure 7b shows the correct interpretation of the helium data, using a baffle bolt spectrum previously used to calculate gas generation [11], but modified to fit the thermal-to-fast ratios obtained from the retrospective dosimetry analysis. Indeed, the predictions match the measurements almost exactly. Such a match was reached without including any boron contribution, and therefore implies that the boron content of the bolt is rather low, perhaps 5 appm or less.

The first observation is that the hydrogen levels vary somewhat from one repeat measurement to the next. Unfortunately, these measurements were made from the small sections left between punched-out microscopy disks, and there is no record of where these measurements correspond with respect to the bolt radius. The hydrogen levels measured in the 1 mm position are consistent, however, with the range of those for the ABB heats shown in Figure 2.

Table 4. Helium and Hydrogen Concentrations in the Tihange Baffle Bolt 2K1R5

Specimen	Material	Mass[a] (mg)	Measured Gas Release (10^{14} atoms)		(appm)[b]	
			^{4}He	^{1}H	^{4}He	^{1}H
1-mm Position	Tihange	0.312	2.426		71.3	
		0.595	4.645		71.6	
		1.005	-	54.0		493
		1.598	-	129		743
25-mm Position	Tihange	0.477	2.784		53.6	
		0.204	1.186		53.8	
		0.264	1.444		50.7	
		1.188		85.0		660[c]
		1.314		233		1620
		0.740		102		1260
		0.181		73.3		3710
		1.295		101		720[c]
		0.809		323		3660
55-mm Position	Tihange	0.448	2.378		48.7	
		0.510	2.726		49.0	
		1.358		553		3740
		1.701		341		1840

[a] Mass of specimen for analysis. Mass uncertainty is ±0.002 mg.
[b] Gas concentration in atomic parts per million (10^{-6} atom fraction) with respect to the total number of atoms in the specimen.
[c] Crucible temperature of ~1000°C instead of ~1200°C.

However, the 25- and 55-mm positions contain concentrations of hydrogen 3 to 7 times that measured in the 1-mm bolt head position, even though the dpa levels are lower. The variations in estimated mid-cycle temperatures of the three positions (320, 343, 333°C for 1, 25, 55 mm, respectively) are not large enough to justify such differences in hydrogen content.

Our current interpretation is that the "extra" hydrogen is stored, possibly as H_2 gas in cavities. As shown in Figure 9, there is approximately 0.2% swelling in the form of cavities in the 25 and 55 mm positions. In the 1 mm position, there is only a few, much smaller density and sizes of cavities, yielding less than 0.01% swelling. Although there is a little more helium in the 1 mm position, most of it must still be in solution or in unresolvable (<1 nm) bubbles and cavities.

Discussion: LWR results

It has been proposed based on the results of other studies [1,12] that helium-nucleated bubbles or voids may allow the storage of hydrogen at LWR-relevant temperatures. From the bolt study, the retention of hydrogen only in those regions where measurable swelling exists lends support for the association of hydrogen with cavities. It is clear, however, that the large levels of hydrogen found in the bolt shank positions cannot be generated from

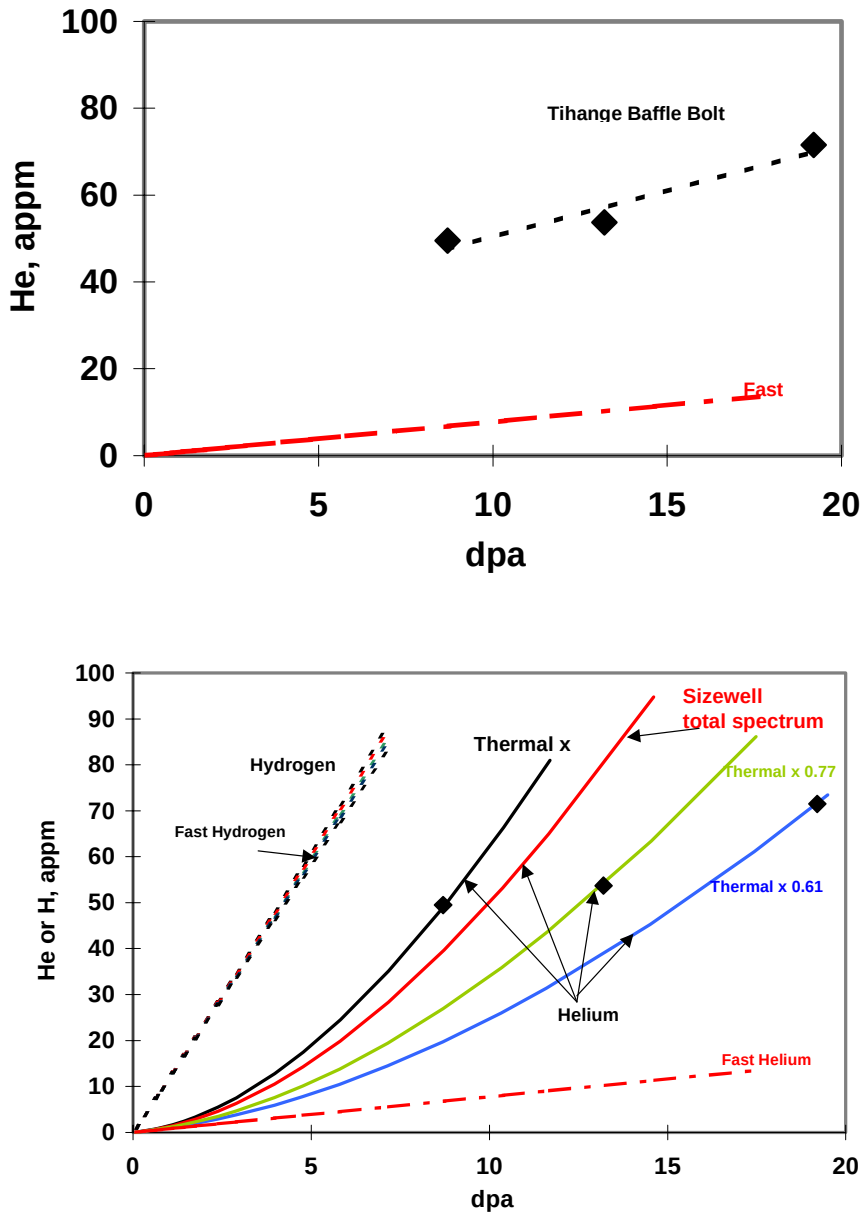

Figure 7. a) Helium measurements from the Tihange baffle bolt, assuming all positions experience the same thermal-to-fast neutron ratio. b) Correct interpretation of helium data showing the contributions of fast neutrons and varying thermal-to-fast ratio. Hydrogen generation is also shown.

Figure 7. b) also shows the transmutant hydrogen levels that would be predicted from the three spectra associated with the three bolt positions. For these relatively low thermal-to-fast ratios, the hydrogen generation is not enhanced significantly in this dpa range by the ^{59}Ni(n,p) reaction. Even more importantly, the predicted transmutant hydrogen levels are rather low (~100-200 appm) compared to the measured values shown in Table 4.

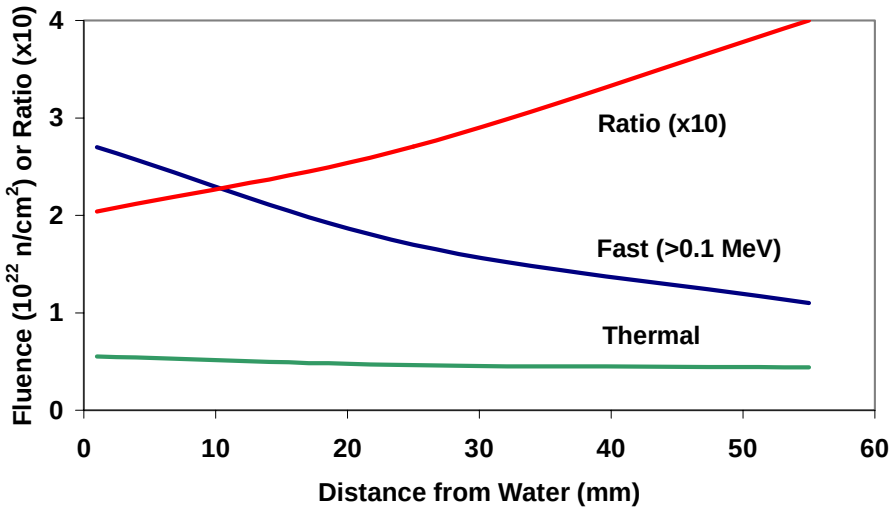

Figure 8. Neutron fluxes and thermal-to-fast ratio for the various positions on the baffle bolt as determined by retrospective dosimetry.

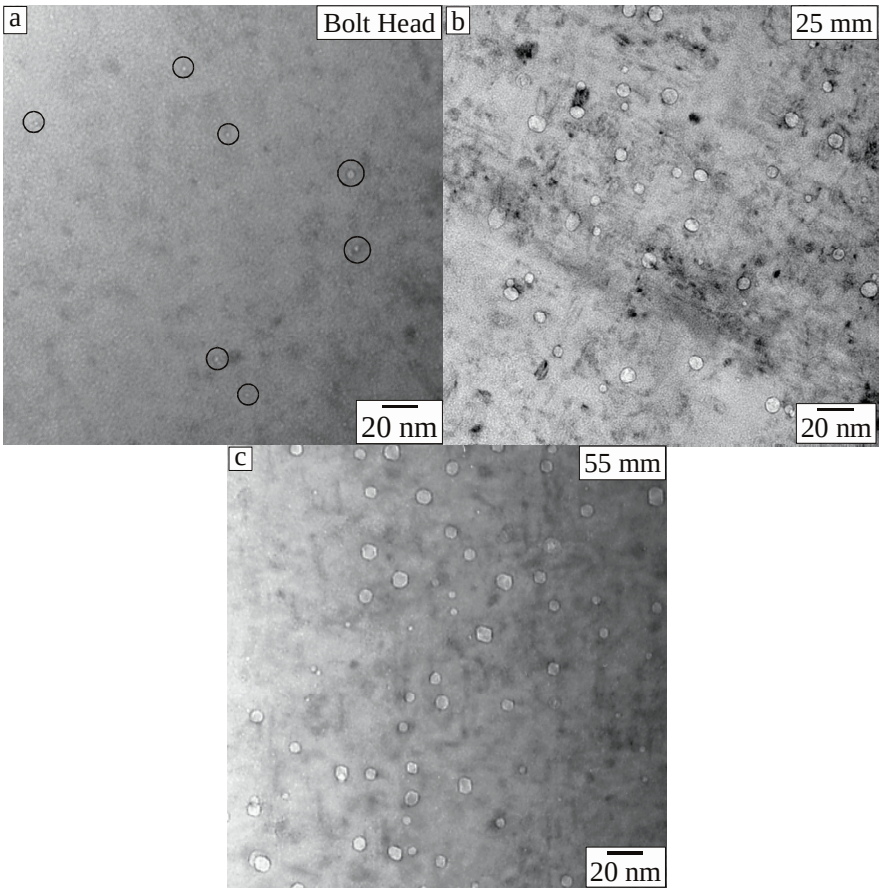

Figure 9. Cavities observed in the baffle bolt sections.

transmutation reactions only, but must result from environmental sources. Note that no cavities exist in the ABB specimens, and cavities exist only in very low densities in the 1-mm position. In both cases the hydrogen levels are correspondingly smaller, lending further credibility to the association between the cavities and retained hydrogen. Several specific questions are raised by these results.

1) Are voids by themselves sufficient to store large amounts of hydrogen?
2) Are there any other examples of significant hydrogen storage in cavities, either bubbles or voids?
3) Have all sources of helium and hydrogen been identified?
4) Is there any evidence for direct association of helium and hydrogen retention?

In order to address these questions the following experiments were performed.

Stainless steels irradiated in FFTF

Three cold-worked 316 stainless specimens irradiated in the FFTF fast reactor were chosen to see if voids *per se* would store hydrogen when hydrogen was generated primarily by transmutation. These specimens were in contact with the sodium coolant. The FFTF core is an oxide-fueled core with a rather soft neutron spectra (mean neutron energy of ~0.5 MeV, and no thermal neutrons), so both the helium and hydrogen generated per dpa are less than that generated by LWR spectra.

Two of the specimens had ~8% swelling, as determined by immersion density measurements and confirmed by electron microscopy [13]. One of these was irradiated to 88 dpa at 400-430°C, and the other to 60 dpa at 550°C. Although the swelling was approximately the same, the cavity densities were very different, at 2.1×10^{21} and 0.15×10^{21} m^{-3}, respectively. Thus, the two specimens had very different void surface areas. The third specimen was part of the 400-430°C irradiation series, but was exposed to only 17.5 dpa, producing only 0.28% swelling. The first two specimens had primarily network dislocations and the low exposure specimen had a Frank loop and network structure.

As shown in Table 5, the measured helium contents in the three samples ranged from 4.99 to 36.8 appm, in good agreement with predictions. Reproducibility between the duplicate analyses averaged ~3%, somewhat higher than the analysis system reproducibility of 0.5%, suggesting some low level of heterogeneity in the helium contents.

Measured hydrogen levels in the irradiated samples ranged from 322 to 570 appm. Given the relatively high irradiation temperatures seen by the samples, however, the fact that hydrogen still exists even at these rather low levels suggests some trapping mechanism may be operating. Reproducibility between the duplicate hydrogen analyses averaged ~38%, which is not inconsistent with the level of variability observed in measurements of our standard hydrogen-containing steel. Most significantly, there was no elevated retention of hydrogen as a function of dislocation structure, total void volume or void surface area.

Model alloys irradiated in FFTF

Four model Fe-15Cr-XNi alloy specimens were irradiated in FFTF in the ^{59}Ni isotopic tailoring experiment in the below-core assembly, at damage levels of either 10.2 or 24 dpa [14,15]. The irradiation temperature was 365°C, which is more prototypic of PWR conditions. Several variables were investigated in this experiment; the effect of nickel level (25 and 45 wt.%) and the effect of He/dpa ratio. The latter was accomplished by doping one half of the alloys with ^{59}Ni extracted from material irradiated in a highly thermalized neutron

Table 5. Measured gas concentrations in 316 stainless steel

Specimen	Mass[a] (mg)	Measured Gas Release (10^{13} atoms)		Gas Concentration (appm)[b]	
		^{4}He	^{1}H	Measured	Average[c]
MAEZ	0.857	4.813	-	5.201	4.99
	0.497	2.569	-	4.786	±0.29
	0.398	-	139	322	-
RAEZ	0.500	19.84	-	36.83	-
	0.620	-	419	626	493
	1.087	-	423	360	±188
PAE7	0.677	12.81	-	17.52	17.6
	0.333	6.343	-	17.64	±0.1
	1.143	-	515	417	570
	0.806	-	629	723	±216

[a]Mass of specimen for analysis. Mass uncertainty is ±0.002 mg.
[b]Gas concentration in atomic parts per million (10^{-6} atom fraction) with respect to the total number of atoms in the specimen.
[c]Mean and standard deviation (1σ) of duplicate analyses.

spectrum. Thus, a side-by-side comparison could be made of the single variable influence of low and high He/dpa rates. The swelling levels were not greatly altered by ^{59}Ni doping, but in general, the swelling was distributed on a much finer scale in the doped alloys. The alloys were swelling 0.2-0.4% at 10.2 dpa and several percent at 24 dpa.

At 10.2 dpa the undoped and doped 25 wt% Ni alloys were previously measured to have 7.1 and 165 appm respectively in the absence of doping. The 45 wt% Ni alloys had 41.6 and 317 appm at 24 dpa. As shown in Table 6, the measured hydrogen levels in the irradiated samples were rather low, ranging from 184 to 545 appm. It should be noted, however, that several hundred appm would be expected to have been present in the materials prior to irradiation.

In effect, there appears to be no storage of excess hydrogen in these specimens, regardless of nickel content, helium level or swelling level.

Ti-modified stainless steel in HFIR

Two stainless steel specimens of US PCA, a modified 316 stainless steel were irradiated in the JP-12 experiment at 400°C in HFIR in the late1980's, with the specimens contained in an aluminum block, which was surrounded by a stainless steel canister, without any possibility to contact water. Microscopy was reported on these and other specimens in 1988 and showed the specimens to be densely packed (~10^{17} cm$^{13)}$ with small (10-20 nm) "helium-filled cavities" [16,17]. The calculated helium level for these specimens was 2835 appm at 33 dpa, produced by the very high thermal-to-fast ratio (~2) in this reactor.

Thirteen years later, identical specimens from the same capsule were retrieved from dry storage and measurements made of the helium and hydrogen. The measured helium levels were 2979 and 3012 appm, within 5% of the calculated values. This agreement provides

Table 6. Hydrogen concentrations in FFTF-MOTA model alloys

Specimen	Material	Mass[a] (mg)	Measured ^{1}H (10^{16} atoms)	Hydrogen Concentration (appm)[b] Measured	Average[c]
ZXLN-2	Fe-15Cr-25Ni 10.2 dpa	3.416	1.53	416	395
		3.478	1.40	373	±30
Z1LN-2	Fe-15Cr-45Ni 10.2 dpa	2.284	0.514	211	293
		2.756	1.10	375	±116
Z3LN-1	Fe-15Cr-25Ni 24 dpa, ^{59}Ni.	3.117	1.70	506	545
		3.422	2.15	583	±54
Z5LN-1	Fe-15Cr-45Ni (d 24 dpa,^{59}Ni.	3.261	0.724	208	184
		3.082	0.522	159	±35

[a]Mass of specimen for analysis. Mass uncertainty is ±0.002 mg.
[b]Hydrogen concentration in atomic parts per million (10^{-6} atom fraction) with respect to the total number of atoms in the specimen. Uncertainty is estimated to be ±20 %.
[c]Mean and standard deviation (1σ) of duplicate analyses.

confidence in our knowledge of the neutron spectrum, and allowed the opportunity to calculate the neutron-induced hydrogen generated, which was predicted to be 884 appm.

Surprisingly, the measured hydrogen values were 3864 and 3790 appm, indicating that the retained hydrogen was more than four times the predicted total generation. In effect, these cavities contain as much hydrogen as helium, assuming that both are largely contained in the cavities. Examination of all details of the experiment revealed no obvious environmental sources of hydrogen strong enough to account for this “excess” hydrogen. While this highly voided microstructure has been clearly storing hydrogen for more than a decade, the major hydrogen source is unknown. Therefore to address the source question in this HFIR experiment, the next experiment was conducted.

Pure metal dosimeters irradiated in HFIR

In the absence of an identifiable environmental source, the possibility of unrecognized transmutant sources must be investigated. Perhaps the various (n,p) and (n,α) cross sections have been underestimated or perhaps some previously unidentified radioisotope source similar to ^{59}Ni is contributing.

Therefore, it was decided that the thin wire dosimeters that were used to determine the spectrum in the JP-12 and follow-on JP-15 experiments were examined. Only the nickel and iron dosimeters were measured. These dosimeters were chosen not only from the 400°C canister used to irradiate the stainless steel specimens discussed above, but also from the 300, 500 and 600°C canisters as well, with dpa levels ranging from 34 to 59 dpa. Some of these dosimeters had not been removed from their original sealed aluminum packets, guaranteeing that the wires had not been exposed to moist air or other potential sources of hydrogen over the last decade.

The hydrogen levels measured for the two metals are shown in Figures 10 and 11. The iron dosimeters showed, with the exception of the 300°C specimen, that the iron specimens had relatively low hydrogen levels, and were comparable to the predicted transmutation level. In such a comparison, however, it is not possible to judge the original hydrogen content or the amount lost during or after the irradiation. In any event, the hydrogen levels were not large enough to identify iron as a transmutant contributor to the "extra" hydrogen. In addition, iron has a relatively high solubility for hydrogen, and the low hydrogen levels tend to support the absence of other environmental sources. The solubility of hydrogen in nickel is known to be lower than that of iron.

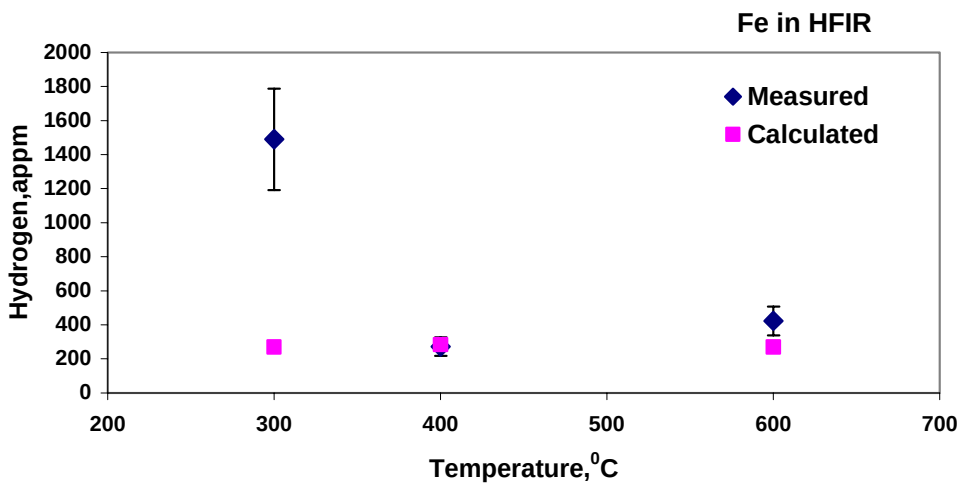

Figure 10. Hydrogen levels measured in pure iron dosimeters from the JP-12 and JP-15 experiments in HFIR.

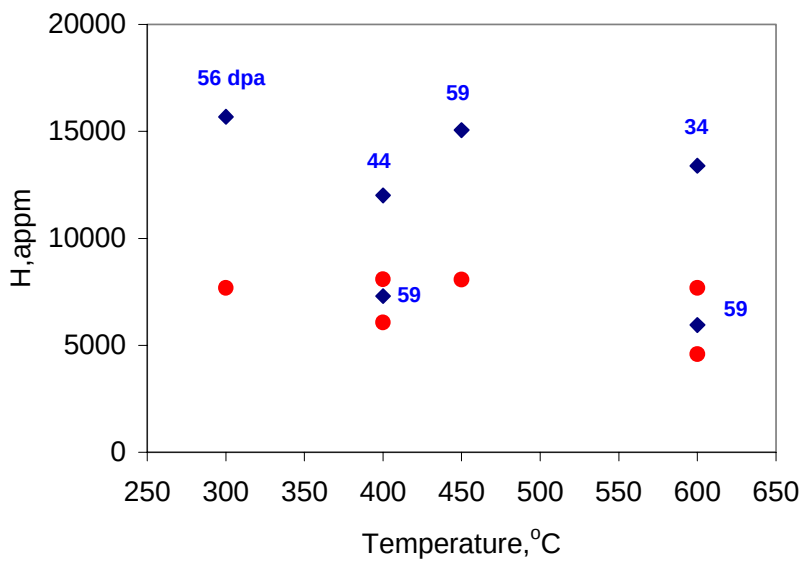

Figure 11. Hydrogen levels measured in pure nickel dosimeters from the JP-12 and JP-15 experiments in HFIR. Diamonds denote measured values; circles denote predictions.

The nickel dosimeters, however, were found to possess very large amounts of hydrogen at levels ranging from 6,000 to 16,000 appm, even at 600°C. Most interestingly, the levels were not strongly dependent on irradiation temperature or dpa level. In effect, these specimens retained more hydrogen than was calculated to have been formed by transmutation. If any diffusional losses have occurred during or after irradiation, the original hydrogen content would have been even larger.

Since nickel demonstrated such an unexpected response with hydrogen, it was decided to measure the helium content as well, since the predictive correlation was developed for total thermal neutron exposures significantly smaller than those explored in this study. Once again, as shown in Figure 12, we are surprised to see the unexpected. It appears measurements are progressively rising with accumulated dpa above the predictive correlation in a manner that is suggestive of another, previously unanticipated, late-term contribution to the helium production.

It therefore appears that nickel or more appropriately, one of its numerous radioactive daughters and granddaughters, may be responsible for both the "excess" hydrogen and helium. Currently, the most likely candidates are thought to be ^{58}Co and ^{65}Zn, since these isotopes are multiple-step in their formation and appear to have favorable Q-values for both (n,p) and (n,α) reactions with thermal neutrons. In fact, ^{65}Zn has a very large thermal

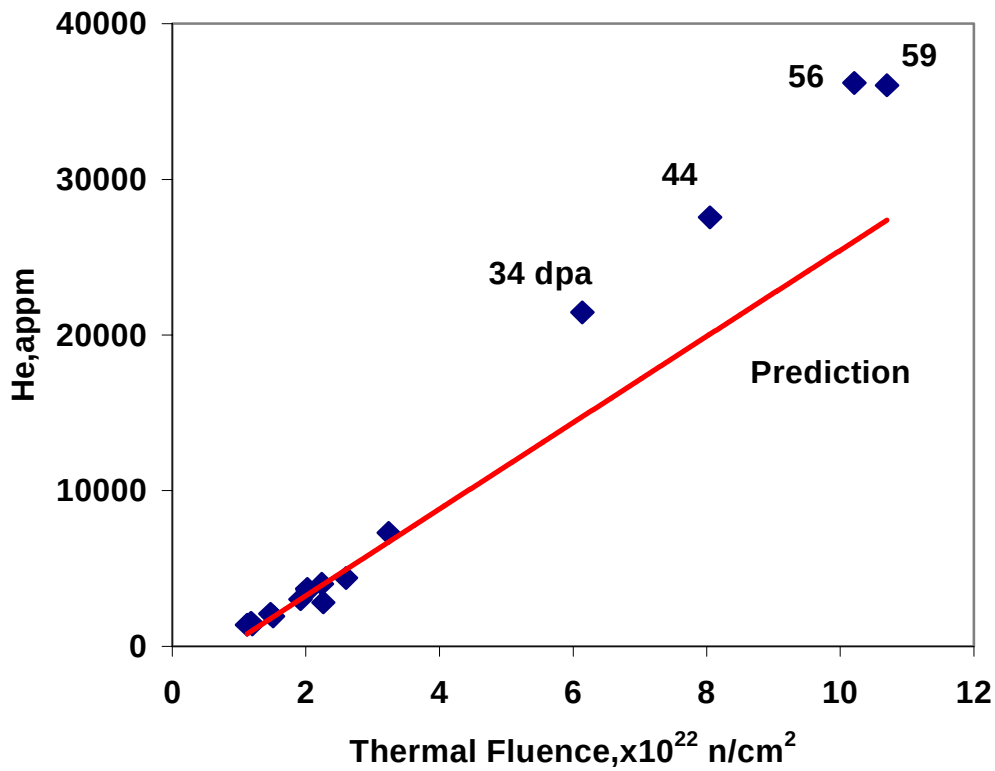

Figure 12. Comparison of measured helium and predictions as a function of thermal fluence. Dpa values are also shown. Data at lower fluences were used to establish the original predictive correlation.

(n,α) cross section of 4.7 barns, so it would not be surprising if it also has a large thermal (n,p) cross section as well [18].

Discussion: Test reactor results

The several sets of FFTF studies show that the accumulation of voidage *per se* is insufficient to store hydrogen if there are not large sources of transmutant or environmental hydrogen to store. On the other hand, the two HFIR studies confirm that the simultaneous presence of voids and strong non-equilibrium concentrations of hydrogen can combine to store hydrogen, regardless of the nature of the hydrogen sources. One additional factor may be the temperature that the specimens experience at the end of the irradiation. In HFIR the temperature quickly drops to the coolant temperature of ~50°C, while in FFTF the sodium coolant in MOTA requires ~15 hours to cool and never drops below ~230°C thereafter.

While the nickel dosimeter results indicate that some nickel daughter or granddaughter isotope may be providing unexpected contributions to helium and especially hydrogen production, this experiment has not shown clearly that the storage in nickel was in cavities. The wires were too small to measure swelling and were destroyed during gas measurement.

However, nickel is well known to exhibit void swelling throughout the 300-600°C range [19-21]. One aspect of swelling in this material is its strong tendency to saturate in swelling at a level that is not only independent of temperature, but also cannot exceed ~8% swelling. If hydrogen is stored in cavities, then perhaps the saturation of both hydrogen and swelling may be directly related.

There is another potential explanation for the dosimeter results, however. If it is allowed that the cumulative uncertainties in the ^{59}Ni(n,α) and ^{58}Co cross sections can be as large as 20-30%, the disparity in helium production might be explained without resort to invoking unidentified transmutant sources. This weakens the argument for an unidentified (n,p) source, however.

Note also that at 300°C the iron dosimeter had an apparently anomalous high hydrogen concentration. It has recently become known that pure iron, especially when cold-worked and irradiated at low temperatures, can exhibit substantial void swelling [21-23]. This suggests that void storage may be in progress in iron at 300°C. Additional measurements are planned to investigate this possibility.

Finally, this line of reasoning leads us back to the possibility of an environmental source of hydrogen to provide the “excess”. Perhaps the source is transmutant hydrogen generated in the large aluminum block that surrounds both the stainless steel specimens and the dosimeter packages. This possibility will be investigated in future studies.

Conclusions

It appears that until exposure levels in excess of typical LWR levels are reached, it is possible to predict the helium production and retention on the basis of alloy composition and neutron flux-spectra. A similar expectation should apply to fusion environments. The prediction of hydrogen retention is more difficult, however, especially since hydrogen appears to become trapped in cavities such as bubbles and voids. Significant trapping in cavities requires strong non-equilibrium concentrations that can arise from either transmutation or environmental sources. The impact of such storage on degradation

processes such as void swelling and irradiation assisted stress corrosion cracking remains to be studied, however.

ACKNOWLEDGEMENTS

The Offices of Basic Energy Sciences, Fusion Energy, and Nuclear Energy, Science and Technology, U.S. Department of Energy provided support for this research under Contract DE-AC06-76RLO 1830. Pacific Northwest National Laboratory is operated for DOE by Battelle Memorial Institute.

REFERENCES

[1] F. A. Garner and L. R. Greenwood, "Neutron Irradiation Effects on Fusion or Spallation Structural Materials: Some Recent Insights Related to Neutron Spectra", in Radiation Effects and Defects in Solids, 144 (1998) 251-283.

[2] L. R. Greenwood, "Neutron Interactions and Atomic Recoil Spectra", J. of Nucl. Mater. 216 (1994) 29-44.

[3] L. R. Greenwood, J. of Nucl. Mater. 116 (1983)137.

[4] L. R. Greenwood and F. A. Garner, J. of Nucl. Mater. 233-237 (1996) 1530.

[5] D. J. Edwards, F. A. Garner, B. A. Oliver and S. M. Bruemmer, "Microstructural Evaluation of a Cold-worked 316SS Baffle Bolt Irradiated in a Commercial PWR", Proc. Of Tenth Intern. Conf. on Environmental Degradation of Materials in Nuclear Power Systems – Water Reactors, Aug. 5 –9, 2001, in press.

[6] H. Farrar and B. M. Oliver, "A Mass Spectrometer System to Determine Very Low Levels of Helium in Small Solid and Liquid Samples", J. Vac. Sci. Technol. A4, 1740 (1986).

[7] B. M. Oliver, J. G. Bradley, and H. Farrar, "Helium Concentration in the Earth's Lower Atmosphere", Geochim. Cosmochim. Acta **48**, 1759 (1984).

[8] B. M. Oliver, F.A. Garner, and L.R. Greenwood, "Quadrupole Mass Spectrometer for the Determination of Low to high Levels of Hydrogen in Irradiated Materials", J. of Nucl. Mater. 283-287 (2000) 1006-1010.

[9] A. Jenssen and L. G. Ljungberg, Final Report: Irradiation Assisted Stress Corrosion Cracking Studies, ABB Atom, SDA-95-1262, (1995).

[10] S. M. Bruemmer, D. J. Edwards, B. W. Arey and L. A. Charlot, "Microstructural, Microchemical and Hardening Evolution in LWR-Irradiated Austenitic Stainless Steel", Proceedings, Ninth International Symposium on Environmental Degradation in Nuclear Power Systems - Water Reactors, (1999) pp. 1079-1087.

[11] F. A. Garner, L. R. Greenwood and D. L. Harrod, "Potential High Fluence Response of Pressure Vessel Internals Constructed from Austenitic Stainless Steels", Proc. Sixth Intern. Symp. on Environmental Degradation of Materials in Nuclear Power Systems - Water Reactors, San Diego, CA. August 1-5, 1993, pp. 783-790.

[12] T. Matsuoka, T. Yonezawa, K. Nakamura, H. Myojin, J. Shimizu and T. Nagata, Proc. Of ICONE-4, Vol. 4, pp. 249-256.

[13] G. L. Hankin, "Radiation-Induced Evolution of Microstructure and Mechanical Properties of Stainless Steels", Ph. D. Thesis, Loughborough University, U.K., 1999.

[14] L. R. Greenwood, F. A. Garner and B. M. Oliver, J. of Nucl. Mater. 212-215 (1994) 492.

[15] F. A. Garner, M. L. Hamilton, L. R. Greenwood, J. F. Stubbins and B. M. Oliver, "Isotopic Tailoring with ^{59}Ni to Study the Effect of Helium on Microstructural Evolution and Mechanical Properties of Neutron Irradiated Fe-Cr-Ni Alloys", Proceedings of 16th ASTM International Symposium on Effects of Radiation on Materials, ASTM STP 1175, Denver, CO, June 22-24, 1992, pp. 921-939.

[16] M. P. Tanaka, S. Hamada, A. Hishinuma and P. J. Maziasz, J. of Nucl. Mater. 155-157 (1988) 801-805.

[17] S. Hamada, P. J. Maziasz, M. P. Tanaka, S. Suzuki and A. Hishinuma , J. of Nucl. Mater. 155-157 (1988) 838-834.

[18] D. W. Kneff, L. R. Greenwood, B. M. Oliver, R. P. Skowronski and E. L. Callis, Radiation Effects 92-93 (1986) 553-556.

[19] F. A. Garner, J. of Nucl. Mater. 205 (1993) 98-117.

[20] F. A. Garner, in Fusion Reactor Materials Semiannual Report for period ending March 31, 1990, DOE/ER-0313/8, pp.125-135.

[21] N. I. Budylkin, E. G. Mironova, V. A. Krasnoselov, S. I. Porollo and F. A. Garner, “Void Swelling and Embrittlement of Pure Iron and Pure Nickel in the BN-350 and BOR-60 Fast Reactors”, to be published in the Proc. of ICFRM-10, Oct, 2001 in Baden-Baden, Germany.

[22] S. I. Porollo, A. M. Dvoriashin, A. N. Vorobyev and Yu. V. Konobeev, J. of Nucl. Mater. 256 (1998) 247.

[23] A. M. Dvoriashin, S. I. Porollo, Yu. V. Konobeev and F. A. Garner, J. of Nucl. Mater. 283-287 (200) 157.